Evaluation of Daily Precipitation Product in China from the CMA Global Atmospheric Interim Reanalysis

Chunxiang LI[1], Tianbao ZHAO[1*], Chunxiang SHI[2], and Zhiquan LIU[2]

1 *Key Laboratory of Regional Climate–Environment Research for East Asia, Institute of Atmospheric Physics, Chinese Academy of Sciences, Beijing* 100029

2 *National Meteorological Information Center, China Meteorological Administration, Beijing* 100081

(Received December 12, 2018; in final form September 23, 2019)

ABSTRACT

The China Meteorological Administration (CMA) recently produced a CMA Global Atmospheric Interim Reanalysis (CRAI) dataset for the years 2007–2016. A comprehensive evaluation of the ability of CRAI to capture the spatiotemporal variability of observed precipitation, in terms of both mean states and extreme indicators over China, is performed. Comparisons are made with other current reanalysis datasets, namely, the ECMWF interim reanalysis (ERAI), Japanese 55-yr reanalysis (JRA55), NCEP Climate Forecast System Reanalysis (CFSR), and NASA Modern-Era Retrospective analysis for Research and Applications version 2 (MERRA2), as well as NCEP Climate Prediction Center (CPC) observations. The results show that, for daily variations of rainfall during warm seasons in eastern China, CRAI and CFSR overestimate the precipitation of the main rain belt, while the overestimation is confined to the area south of 25°N in JRA55 but north of 24°N in MERRA2; whereas ERAI tends to underestimate the precipitation in most regions of eastern China. Two extreme metrics, the total amount of precipitation on days where daily precipitation exceeds the 95th percentile (R95pTOT) and the number of consecutive dry days (CDDs) in one month, are examined to assess the performance of reanalysis datasets. In terms of extreme events, CRAI, ERAI, and JRA55 tend to underestimate the R95pTOT in most of eastern China, whereas more frequent extreme rainfall can be found in most regions of China in both CFSR and MERRA2; and all of the reanalyses underestimate the CDDs. Among the reanalysis products, CRAI and JRA55 show better agreement with the observed R95pTOT than the other datasets, with fewer biases, higher correlation coefficients, and much more similar linear trend patterns, while ERAI stands out in better capturing the amount and temporal variations of the observed CDDs.

Key words: China Meteorological Administration (CMA), the CMA Global Atmospheric Interim Reanalysis (CRAI), precipitation, daily

Citation: Li, C. X., T. B. Zhao, C. X. Shi, et al., 2020: Evaluation of daily precipitation product in China from the CMA global atmospheric interim reanalysis. *J. Meteor. Res.*, **34**(1), 117–136, doi: 10.1007/s13351-020-8196-9.

1. Introduction

China is the most populated nation (Piao et al., 2010) and one of the fastest-growing economies in the world (Hubacek et al., 2007). It is characterized by complex topography and heterogeneous climate (Gao et al., 2008). Since China is experiencing rapid industrialization, urbanization, growing agricultural demand, and environmental degradation, a variety of problems have challenged the management and utilization of China's water resources (Varis and Vakkilainen, 2001). Therefore, reliable, long-term, and relatively high-resolution precipitation datasets are essential for natural process modeling, hydrometeorological analysis and forecasting, and monitoring of climatic variations and changes (Kucera et al., 2013; Kirschbaum et al., 2017).

A rain gauge is a mechanical and simple ground-based measurement tool for rainfall, and provides highly accurate precipitation datasets for various climatological and hydrological applications (Kidd, 2001). However, the

Supported by the China Meteorological Administration Special Public Welfare Research Fund (GYHY201506002) and National Natural Science Foundation of China (41790475, 41675094, and 41605066).

*Corresponding author: zhaotb@tea.ac.cn.

distribution of rain gauges is uneven across the country. The ground-based measurement networks in China are mainly distributed in southeastern and central China, while the spatial distribution of stations in other regions are relatively sparse. Additionally, observations are prone to severe underestimation of precipitation, which is amplified in cases of solid precipitation and over mountainous areas (Rasmussen et al., 2012; Isotta et al., 2015). With advanced infrared and microwave instruments, satellite observations make up for these deficiencies by providing coverage that is more temporally complete and spatially homogeneous for vast areas of the globe (Kidd and Levizzani, 2011). However, satellite-related datasets have limitations in terms of their short history and their retrieval approaches, their relative insensitivity to light rainfall events, and their tendency to fail over snow- and ice-covered surfaces, making them susceptible to systematic biases (Ferraro, 1997; Dai et al., 2007; Ebert et al., 2007; Kidd and Levizzani, 2011).

Precipitation estimates from atmospheric reanalysis data with good spatial and temporal continuity provide a potential alternative in regions where conventional in situ precipitation measurements are not readily available. However, because reanalysis data contain uncertainties resulting from the forecast model, data assimilation, and data sources used, it is fundmental to evaluate the quality of reanalysis products in representing weather and climate variations (Trenberth and Guillemot, 1998; Lin et al., 2014). In China, many studies have assessed the performance of reanalysis data in reproducing the diurnal cycle, interannual variation, climatology, and long-term trend of observed precipitation (e.g., Dai et al., 2011; Wang and Zeng, 2012; Chen et al., 2014; Lin et al., 2014). For example, through a preliminary comparison with observational data, Zhao and Fu (2006) found that ECMWF 40-yr reanalysis (ERA-40) and NCEP/NCAR reanalysis 2 (NCEP-2) were able to reflect the temporal and spatial distribution of precipitation but showed regional variation. Ma et al. (2009) evaluated precipitation from ERA-40, NCEP-1, NCEP-2, Climate Prediction Center (CPC) Merged Analysis of Precipitation version 1 (CMAP-1), CMAP-2, and Global Precipitation Climatology Project version 2 (GPCP-2) with ground-based measurements in China and concluded that CMAP-1 and GPCP-2 generally had better correspondence with adjusted observational precipitation. Chen et al. (2014) found that four reanalyses [Japanese 55-yr reanalysis (JRA55), ECMWF interim reanalysis (ERAI), NCEP Climate Forecast System Reanalysis (CFSR), and NASA Modern-Era Retrospective analysis for Research and Applications (MERRA)] reproduced well the rainfall diurnal cycle over East Asia in terms of the contrast over large-scale terrain, the evolution during summer, and its interannual variability.

Additionally, some comparisons of extreme precipitation according to reanalysis data have been carried out in previous studies from a global perspective and for several regions, including China. For instance, Sillmann et al. (2013) highlighted the large spread in absolute values of precipitation extremes between different reanalysis products, comparable to the spread between different climate models from CMIP5. Donat et al. (2014) found that the extreme precipitation patterns and time series from reanalyses showed lower agreement with observations than for extreme temperatures, but generally still correlated significantly. However, some spatial variations have not been considered in China, and further analyses are needed, especially in assessing the performance of the China Meteorological Administration (CMA) Global Atmospheric Interim Reanalysis (CRAI) against that of previous reanalyses.

Recently, the CMA released its first reanalysis, called the CMA 40-yr Global Reanalysis (abbreviated to CRA-40). It was designed to provide global land surface information from as early as 1979 that includes ground temperature, soil moisture, precipitation, etc. Subsequently, a 10-yr interim product (i.e., CRAI), with a horizontal resolution of approximately 34 km and temporal resolution of 6 h, has been produced. The present study comprehensively assesses the ability of CRAI to capture the observed mean state and spatiotemporal variability of precipitation, as well as extreme precipitation indicators, over China. More specifically, comparisons with observations are provided, along with an examination of how well different reanalyses agree with each other, and a determination of whether there are significant regional or seasonal variations in the discrepancies between the models.

Following this introduction, Section 2 describes the observational and reanalysis datasets employed in the study. Comparisons of the characteristics of precipitation from 2007 to 2016, including the climatology of daily precipitation and extreme indicators as well as the related atmospheric circulation features, are presented in Section 3. Finally, Section 4 summarizes our findings and draws the conclusions.

2. Datasets and methods

This study utilizes the daily precipitation from the following reanalysis datasets: CRAI, ERAI (Dee et al., 2011), JRA55 (Kobayashi et al., 2015), CFSR (Saha et

al., 2010), and MERRA2 (Reichle et al., 2017) (see Table S1 in the online supplementary material for further details on these reanalysis datasets). The real-time precipitation dataset derived from the NCEP's CPC (Xie et al., 2010), covering 2007–2016, is also used, as an observational reference for the evaluation. This product is a gauge-based analysis of daily precipitation constructed over the global land areas, at a 0.5° × 0.5° spatial resolution. It is used as a baseline for evaluation in this study because it combines all ground-based information sources. There are also other observational products available for regions of interest, such as Global Precipitation Climatology Center (GPCC) gauge data (Rudolf et al., 2010) and the East Asia daily analysis data (Xie et al., 2007); however, these products do not cover the entirety of 2007–2016.

Two indicators are used in this study owing to their usefulness in representing dry or wet conditions (Alexander et al., 2006; Moberg et al., 2006; Zhang et al., 2011). The indicator for wet conditions is R95pTOT, which denotes the monthly amount of precipitation when daily precipitation is greater than the 95th percentile of daily precipitation (R95p); while the index for dry conditions is CDD, which is the maximum number of consecutive dry days (CDDs) when daily rainfall amounts are less than 1 mm (in units of days per month). Owing to the lack of observational data on vertical wind speed and specific humidity, we only analyze the water vapor flux from the five reanalyses to give a general explanation for the difference in precipitation between CRAI and the other four reanalyses. The water vapor flux is calculated as an integral over the atmospheric column for the eastward and northward components retrieved from 20 pressure levels between 300 and 1000 hPa (Trenberth, 1991; Zhou, 2003). A description of the calculation of the moisture flux and its divergence (Chen, 1985) is given in the online supplemental material.

All the precipitation datasets have been converted from subdaily to daily timescales (mm day^{-1}). Both the gauge-based and reanalysis precipitation products have been interpolated to common grid cells with a horizontal resolution of 0.5° × 0.5° for comparison. It should be noted that, given the difference in horizontal resolution between the different grids, some information might be lost in the re-gridding. To assess the performances of the reanalyses, the bias, relative bias, root-mean-square error (RMSE), Pearson correlation coefficient, and empirical orthogonal function (EOF) analysis are used as statistical metrics in this study (Chen et al., 2013; Zhao and Yatagai, 2014; Guo et al. 2016). The details for calculating these statistics are provided in Table 1.

3. Results

3.1 *Comparison of 10-yr mean daily precipitation*

3.1.1 *Spatial distribution*

First, we briefly compare the climatological precipitation characteristics of China among the reanalyses. More detailed comparisons, as well as validations of the mean precipitation of China, can be found in Su et al. (1999) and Ma et al. (2009). Overall, the precipitation distribution in China is characterized by a northwest-to-southeast increase in the annual and half-year mean precipitation (Ding and Chan, 2005; Gao et al., 2006). All of the reanalysis products capture this spatial pattern (figure omitted), and the pattern correlations are approximately 0.9 (Table 2). Figure 1 displays the 10-yr mean differences of daily precipitation between each of the reanalysis products and the CPC precipitation for the annual, warm half-year (April–September), and cold half-year (October–March) periods from 2007 to 2016. The figure illustrates that the bias is much greater in warm seasons than in cold seasons, and is spatially greater in southern areas than in northern parts, especially in the northeast. Given the association with the East Asian monsoon (Zhou et al., 2010), the warm seasons and southern regions correspond to high precipitation amounts (Shen et al., 2010), resulting in large differences (Luo et al., 2013; Sun et al.,

Table 1. Metrics used in the evaluation of precipitation data. The observations and reanalysis data are denoted as x and y, respectively. The sample means for x and y are defined as $\bar{x} = \frac{1}{N}\sum_{i=1}^{N} x_i$, and $\bar{y} = \frac{1}{N}\sum_{i=1}^{N} y_i$, respectively

Measure	Expression	Description
Bias	$\frac{1}{N}\sum_{i=1}^{N}(y_i - x_i)$	Range [−∞, +∞], best value = 0
Relative bias	$\frac{\bar{y}-\bar{x}}{\bar{x}}\times 100\%$	Range [−∞, +∞], best value = 0
Pearson correlation coefficient (R)	$\frac{\sum_{i=1}^{N}(x_i-\bar{x})(y_i-\bar{y})}{\sqrt{\sum_{i=1}^{N}(x_i-\bar{x})^2}\sqrt{\sum_{i=1}^{N}(y_i-\bar{y})^2}}$	Range [−1, 1], best value = 1
Root-mean-square error (RMSE)	$\sqrt{\frac{1}{N}\sum_{i=1}^{N}(y_i - x_i)^2}$	Range [0, +∞], best value = 0

Table 2. Pattern correlation coefficients and reanalysis biases for 10-yr mean of daily precipitation for annual, warm half-year (April–September), and cold half-year (October–March) periods during 2007–2016 in China between the observational data and reanalysis datasets (CRAI, ERAI, JRA55, CFSR, and MERRA2)

		CRAI	ERAI	JRA55	CFSR	MERRA2
Pattern correlation	Annual	0.89	0.85	0.91	0.90	0.85
	Warm half-year	0.88	0.84	0.90	0.88	0.82
	Cold half-year	0.88	0.82	0.90	0.89	0.88
Bias (mm day^{-1})	Annual	0.29	0.18	0.46	0.81	1.00
	Warm half-year	0.45	0.27	0.64	1.19	1.54
	Cold half-year	0.14	0.09	0.29	0.42	0.45

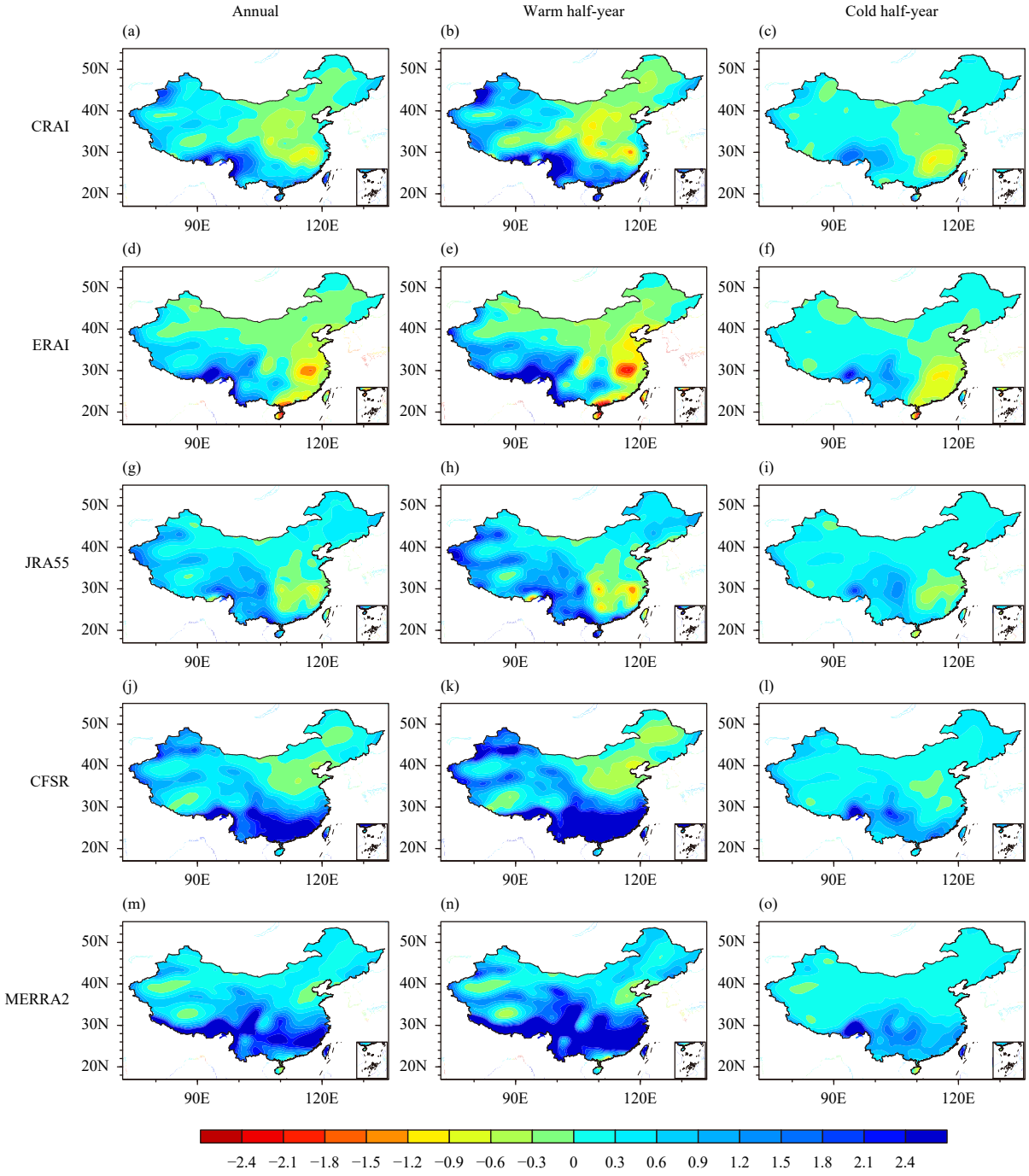

Fig. 1. Distributions of 10-yr mean differences of daily precipitation (shading; mm day^{-1}) between the reanalysis datasets: (a–c) CRAI, (d–f) ERAI, (g–i) JRA55, (j–l) CFSR, and (m–o) MERRA2 and the observations for (left panels) annual, (middle panels) warm half-year (April–September), and (right panels) cold half-year (October–March) periods during 2007–2016.

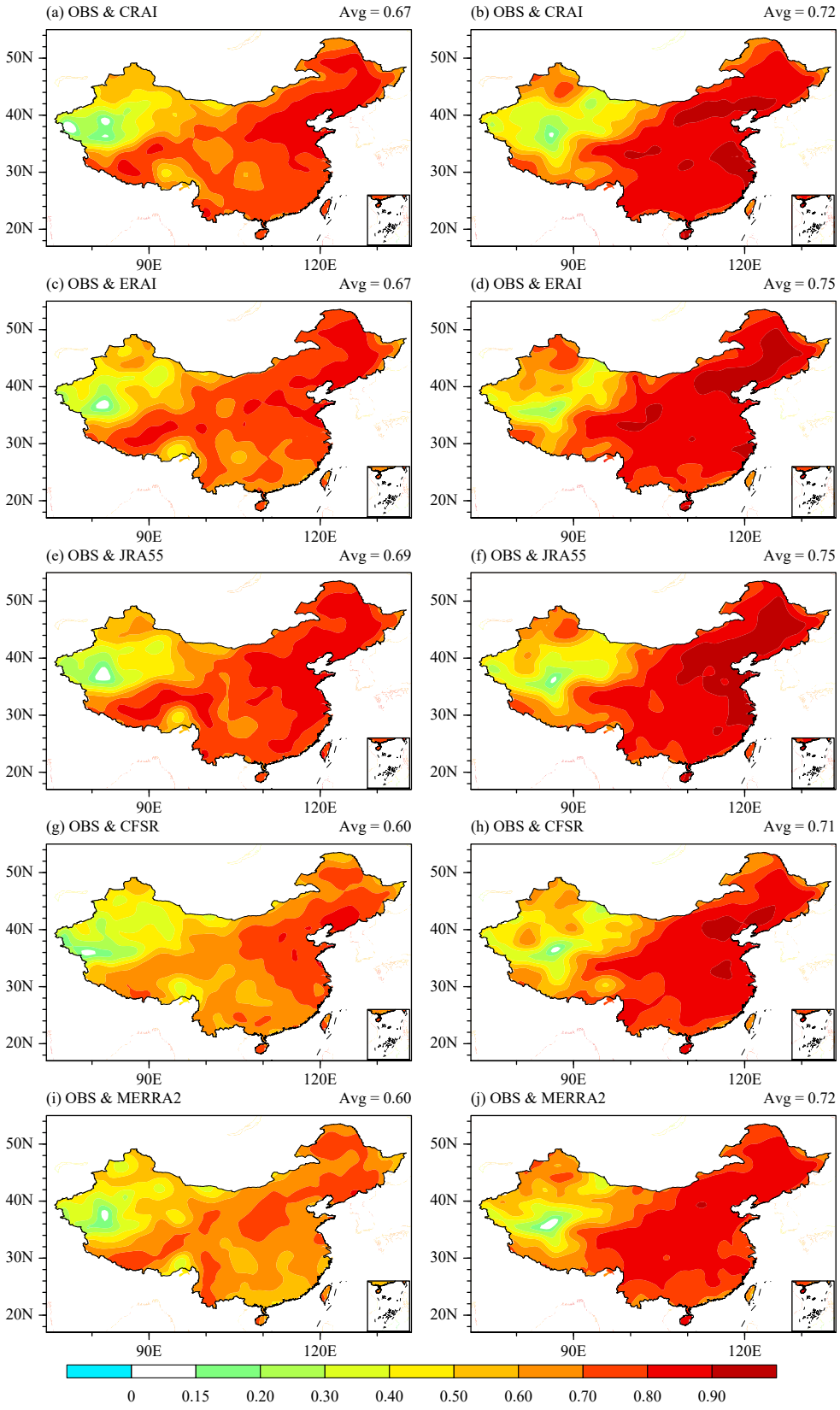

Fig. 2. Serial correlation coefficients (shading) of the 10-yr mean daily precipitation between the observations (OBS) and reanalysis datasets: (a, b) CRAI, (c, d) ERAI, (e, f) JRA55, (g, h) CFSR, and (i, j) MERRA2 for (left panels) warm half-year (April–September) and (right panels) cold half-year (October–March) periods during 2007–2016. The values greater than 0.15 are significant at the confidence level of 95% with a sample number of 183. The average value (Avg) of the serial correlation coefficients is indicated on the top right of each panel.

2014). Among the five products (Table 2), the precipitation amounts from ERAI have a lower bias (0.09–0.18 mm day^{-1}) but correlate slightly less with spatial patterns against the observational data (R = 0.82–0.85) than do those of the other reanalyses (R = 0.82–0.91). The bias in MERRA2 exceeds 1.54 and 0.45 mm day^{-1} for the national average in the warm and cold seasons, respectively. The larger discrepancies in MERRA2 are partly driven by the large seasonal bias across the southern regions.

Figure 2 illustrates the temporal correlation coefficients (R) of the 10-yr mean daily precipitation between the CPC observational data and the reanalyses for warm half-year and cold half-year periods. This figure shows that performances of the five reanalysis datasets at representing temporal variations of daily precipitation are better in the eastern half of the country, especially the northeastern portions, than in the western half of the country, and are better for the cold half-year than for the warm half-year. Elsewhere, correlation coefficients are mostly lower than 0.15 over Northwest Tibetan Plateau (TP), where precipitation amounts are already small. This might be due to large uncertainties in both the gauge-based analysis and the reanalyses. Among the five reanalysis products, JRA55 also stands out in capturing the temporal variations in precipitation in both the warm and cold seasons, with a national average R of 0.69 and 0.75, respectively.

3.1.2 *Temporal variation*

In this section, we analyze the fields of climatological daily precipitation by calculating the time series of the 10-yr (2007–2016) mean daily precipitation for the 366 calendar days for all grids. We first compare the national average time series of observations with the five reanalyses based on statistics constructed from 5-day running means using daily estimates (Fig. 3). For all the reana-

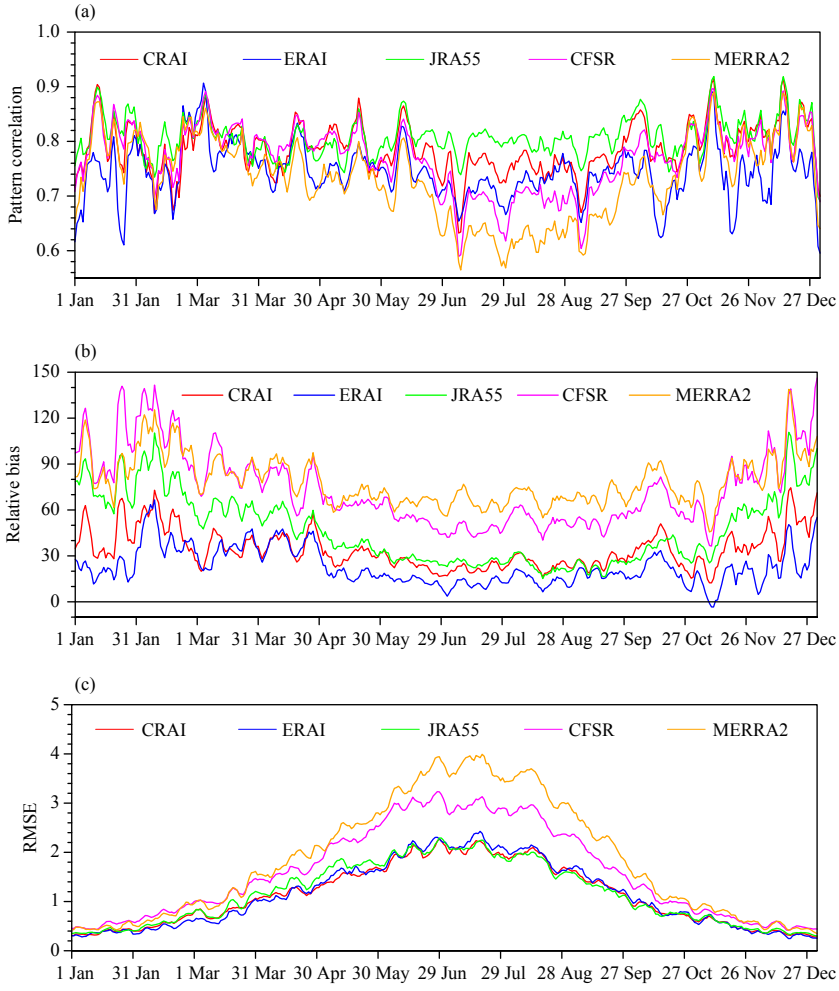

Fig. 3. Time series of (a) pattern correlation coefficient, (b) relative bias (%), and (c) RMSE for the 10-yr mean daily precipitation between the reanalysis datasets (CRAI, ERAI, JRA55, CFSR, and MERRA2; denoted by color lines) and the observations from 1 January to 31 December during 2007–2016. The pattern correlation coefficients are calculated over the domain of China. The time series is smoothed by using 5-day running means for clarity of display.

lyses, both the spatial correlation and relative bias are smaller for the warm season than for the cold season. In contrast, it can be seen that the RMSE has higher values during the warm season. Since the relative bias (RMSE) will often have lower (higher) values when precipitation is higher, it is important to state that these results cannot be attributed to temporal differences, but do provide a diagnosis regarding performances of the products. CRAI, ERAI, and JRA55 closely align with the observations in China for all three statistics. The RMSE values are quite similar for each of them (Fig. 3c), while ERAI has better bias characteristics (Fig. 3b) and JRA55 has consistently higher correlations throughout most of the 12-month comparison period (Fig. 3a).

The daily precipitation rate is classified into four grades according to the criteria defined by the CMA (Committee for the Verification of Terms in Atmospheric Sciences, 2009): light (1.0–9.9 mm day^{-1}), moderate (10.0–24.9 mm day^{-1}), heavy (25.0–49.9 mm day^{-1}), and extreme (≥ 50.0 mm day^{-1}) precipitation. Here, we examine the frequency of daily precipitation occurrence to understand how well the reanalysis products match the observed daily precipitation. The distribution of daily precipitation rates among the observational data and reanalyses from all of the grid points within China from 2007 to 2016 is depicted as a histogram in Fig. 4. For precipitation intensities between 1.0 and 18 mm day^{-1}, all of the reanalysis products have the higher frequency of rainfall occurrence compared to the observational data. For precipitation rates higher than 25 mm day^{-1}, however, three of the five reanalysis products (CRAI, ERAI, and JRA55) detect the lower frequency of rainfall occurrence compared to the observational data, indicating a suppression of heavy and extreme precipitation. Additionally, it is found that the overestimation from CRAI, ERAI, and JRA55 (Fig. 1) is mainly caused by the overestimation of the light and moderate grades. Meanwhile, both CFSR and MERRA2 tend to overestimate the observed precipitation in all categories from light to extreme ranges. Note that CRAI most closely matches the observed distribution of precipitation rates for the 8–25 mm day^{-1} range, suggesting that the best representation of moderate precipitation is found in CRAI.

The evolution of the warm-season precipitation belt from the south to the north in eastern China is also investigated. Figure 5 shows the time–latitude cross-sec-

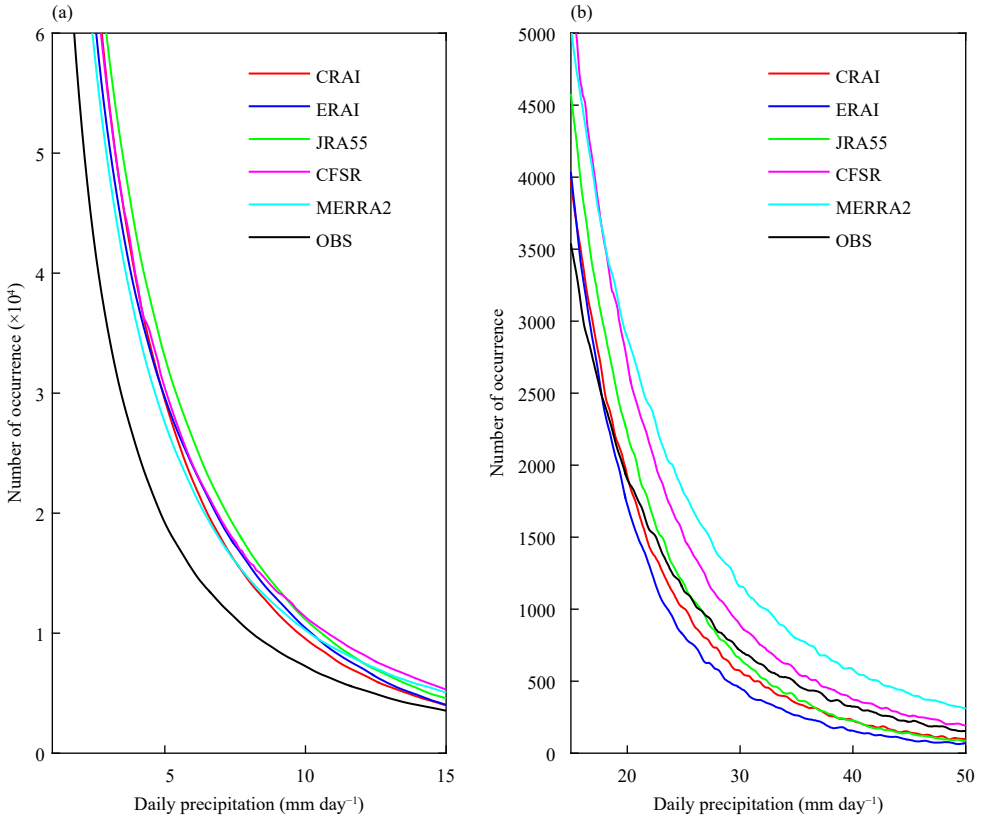

Fig. 4. Histograms of the daily precipitation from all 0.5° grid boxes within China for the CRAI (red), ERAI (blue), JRA55 (green), CFSR (magenta), MERRA2 (cyan), and observations (OBS; black) with the precipitation intensity range of (a) 0–15 and (b) 15–50 (mm day^{-1}) during 2007–2016. The *y*-axis denotes the number of precipitation rate occurrences. The precipitation rate is binned at 0.15 mm day^{-1} intervals. Note the scale change on the *y*-axis between (a) and (b).

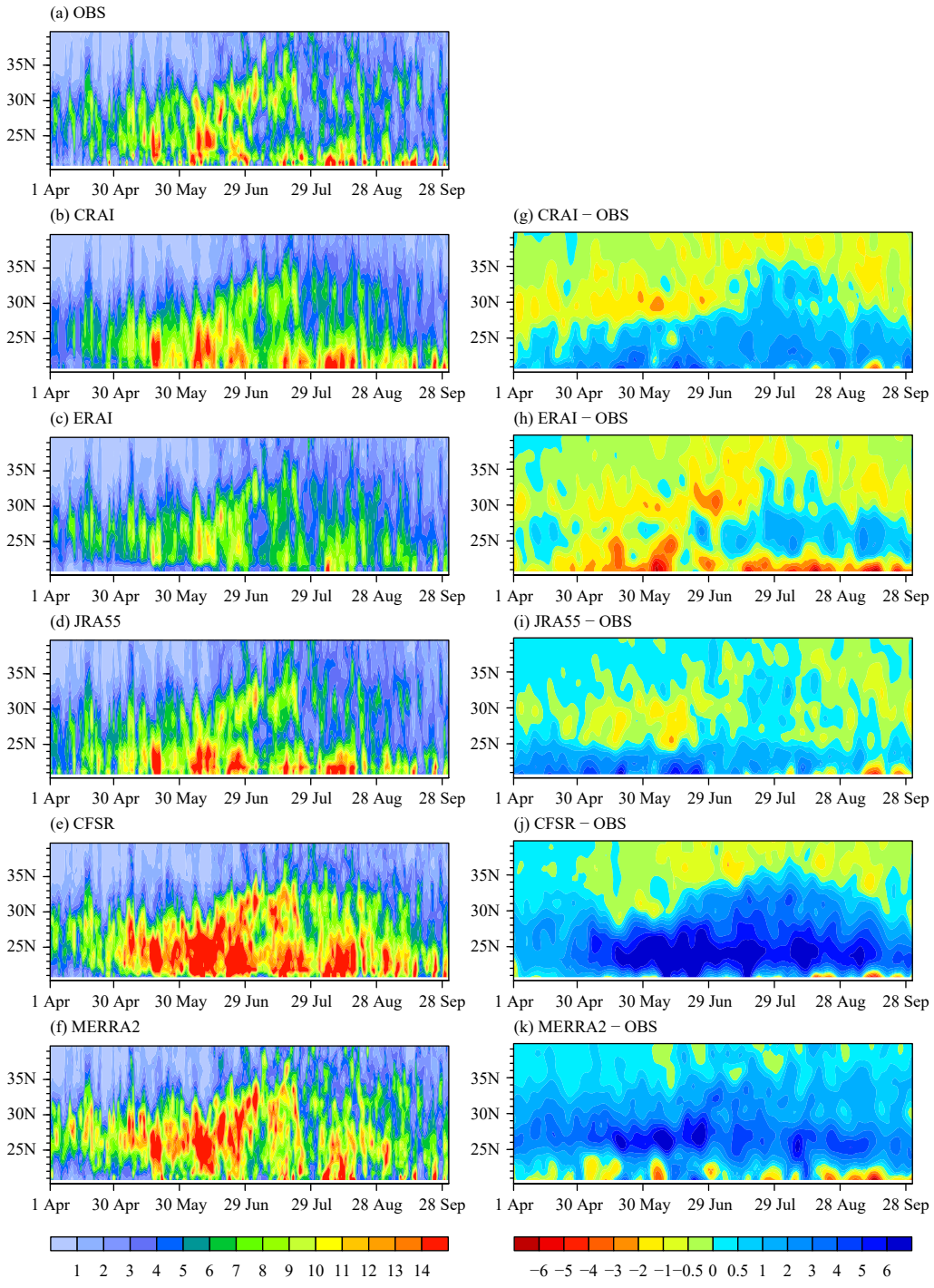

Fig. 5. Time–latitude cross-sections of 10-yr mean daily precipitation (shading; mm day^{-1}) averaged over 105°–120°E (East China) from (a) the observations (OBS), (b) CRAI, (c) ERAI, (d) JRA55, (e) CFSR, (f) MERRA2, and (g–k) the corresponding differences between the reanalysis datasets and OBS from 1 April to 30 September during 2007–2016.

tion of 10-yr mean daily precipitation averaged over 105°–120°E for the observational data and the reanalyses from 1 April to 30 September during 2007−2016. The observational data show that persistent rainfall occurs between 25° and 30°N in early April, and then the rainfall amount gradually increases and expands southward to 20°N in mid-May. After early June, heavy rain with a central value of 12 mm day^{-1} occurs near 22°N and migrates remarkably northward towards 35°N at the end of July, corresponding to the Meiyu rain band and its seasonal migration. Subsequently, the zonally oriented belt of heavy rainfall retreats southward to an area south of 25°N, where the landfall of typhoons introduces abundant fresh water (Gao and Xu, 1962; Ding, 1992,

1994). All of the reanalyses capture the exact timing and location of the rainfall band, as well as the seasonal migration of the precipitation band in eastern China, reasonably well (Figs. 5b–f). However, all of the reanalyses except ERAI tend to overestimate the amount of precipitation in South China. That is, both CFSR and CRAI exhibit stronger precipitation in the rain belt during the whole period, whereas overestimation is confined to south of 25°N in JRA55 but to the north of 24°N in MERRA2. ERAI, except for a slightly stronger rainfall predicted between 23° and 28°N after late June, displays an underestimation in most regions of eastern China, es-

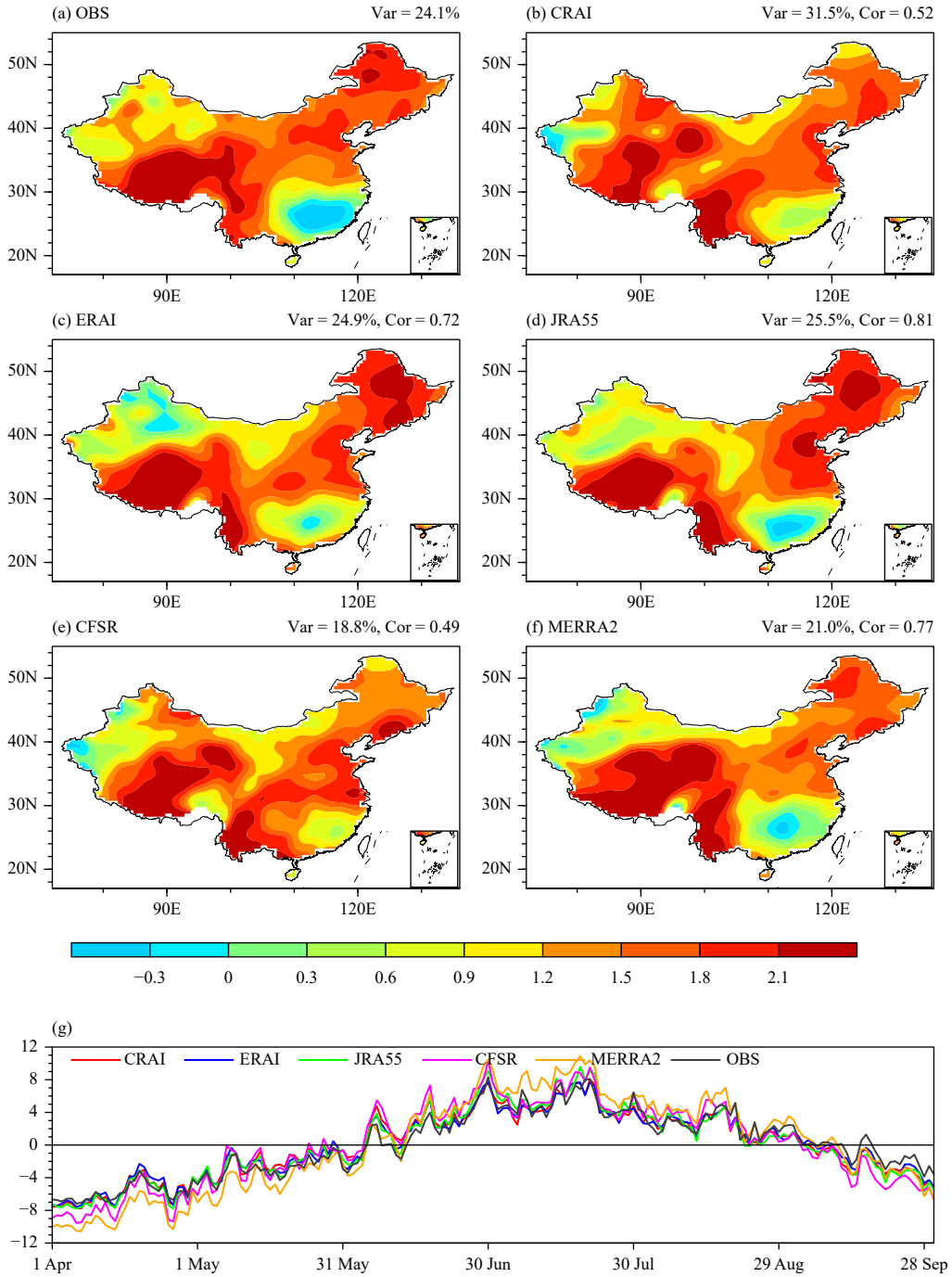

Fig. 6. (a–f) Spatial (shading) and (g) temporal (black and color lines) patterns of the first leading EOF mode (EOF1) of the 10 yr-mean daily precipitation over China from 1 April to 30 September during 2007–2016 from (a) the observations (OBS), (b) CRAI, (c) ERAI, (d) JRA55, (e) CFSR, and (f) MERRA2. Red (blue) areas in (a–f) are wet (dry) for a positive pattern correlation coefficient. The percentage of variance (Var) explained by the EOF1 and the pattern correlation coefficient (Cor) between the reanalysis data and OBS are shown on the top right of the corresponding panel. Note that all the correlation coefficients are statistically significant at the 95% confidence level.

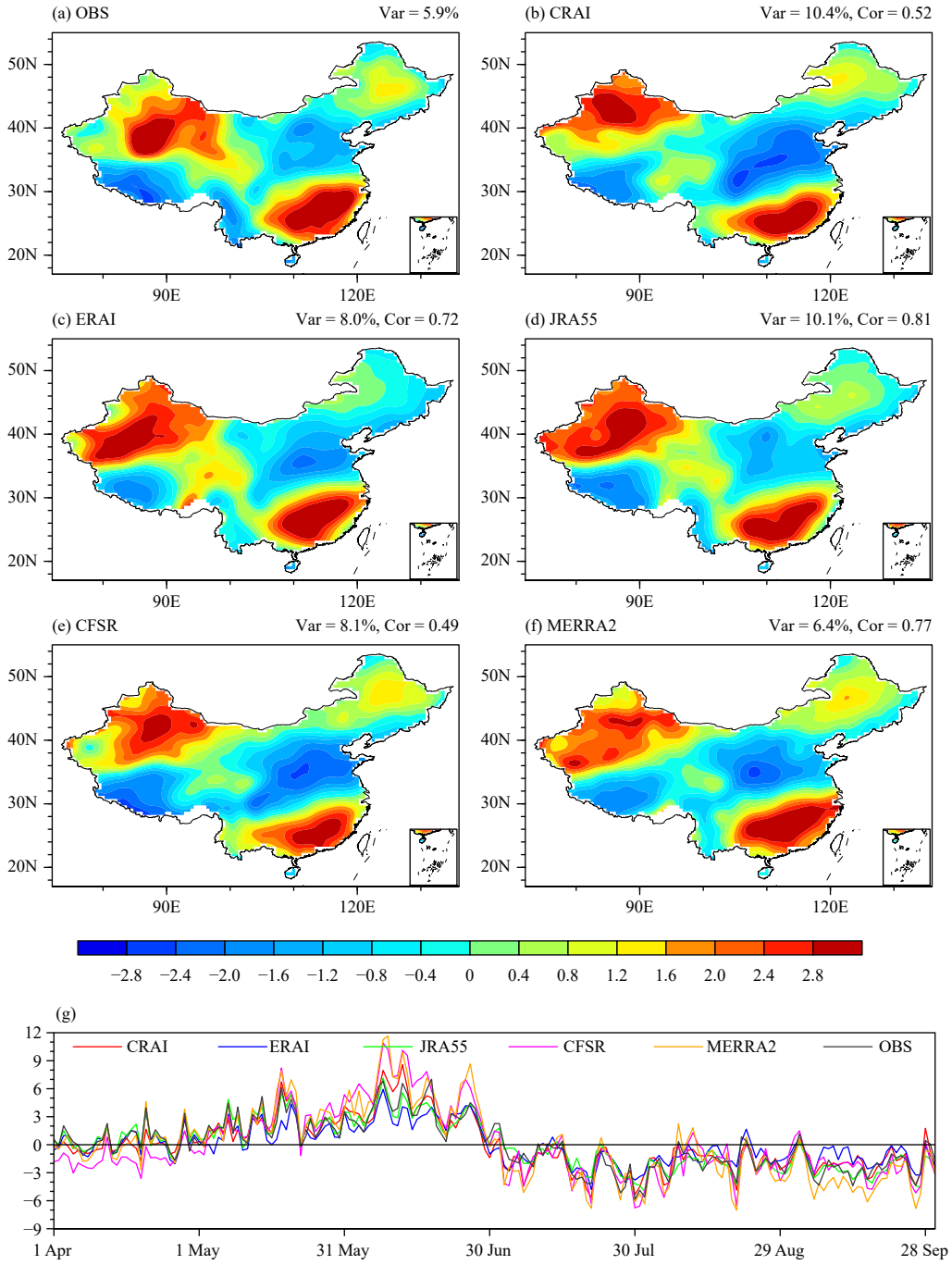

Fig. 7. As in Fig. 6, but for the second EOF mode (EOF2).

pecially in the southern portions of South China during the entire period and in the lower reaches of the Yangtze River before late July.

3.1.3 *EOF analysis of warm half-year precipitation*

To assess the seasonal and intraseasonal variability of precipitation as represented in the reanalyses and observational data, we apply an EOF analysis. Using the results from the EOF analysis of the 10-yr mean seasonal cycle from 1 April to 30 September (Figs. 6 and 7), the spatial characteristics, including the shape, orientation and location of the rainfall area, of daily rainfall in China are investigated. The first two leading EOF modes of the five reanalyses and the observational data account for 41.9%, 32.9%, 35.6%, 26.9%, 27.4%, and 30.0% of the total variance, respectively.

It can be seen that positive anomalies are dominant in the first EOF mode (EOF1), particularly in the northeast and southwest of China, whereas negative anomalies are

confined to South China (Fig. 6d). Associated with temporal coefficients (Fig. 6e), this mode corresponds to above-normal rainfall in South China before early-June and after August, which refers to the onset of the pre-flood and post-flood seasons of South China, respectively. Overall, the agreement is good between the reanalyses and observational data (pattern correlation coefficients: 0.49–0.81; PCs correlated at 0.95–0.99), but regional differences exist. For instance, compared to the observational data, both CRAI and CFSR depict an opposite sign of the seasonal precipitation variability in South China, showing in-phase changes across the whole of China.

The second EOF mode (EOF2) features a "positive–negative–positive" meridional pattern in eastern China, but displays a dipole pattern in western China (Fig. 7d). Associated with the temporal coefficient curve (Fig. 7e), we can see that the main abundant rainfall areas are located in southern, northeastern, and northwestern China, whereas the deficient rainfall areas are located in southwestern and northern China before late June. Hereafter, an opposite sign is found, depicting a north–south migration of the precipitation largely modulated by the monsoon circulations. The corresponding modes from all of the reanalyses capture these features reasonably well (pattern correlation coefficients: 0.49–0.81; PCs correlated at 0.87–0.96), but slightly underestimate the variability in southwestern and northeastern China (Figs. 7a–c). Moreover, there is a substantial overestimation of the seasonal variability in the middle and lower basins of the Yellow River in CRAI and CFSR (Figs. 7b, e). Overall, among the reanalyses, JRA55 outperforms the other four reanalysis products in capturing the structure and variability of precipitation in warm seasons in eastern China.

3.2 *Comparison of extreme events*

In this section, we evaluate the performance of reanalyses in capturing the behavior of extreme precipitation

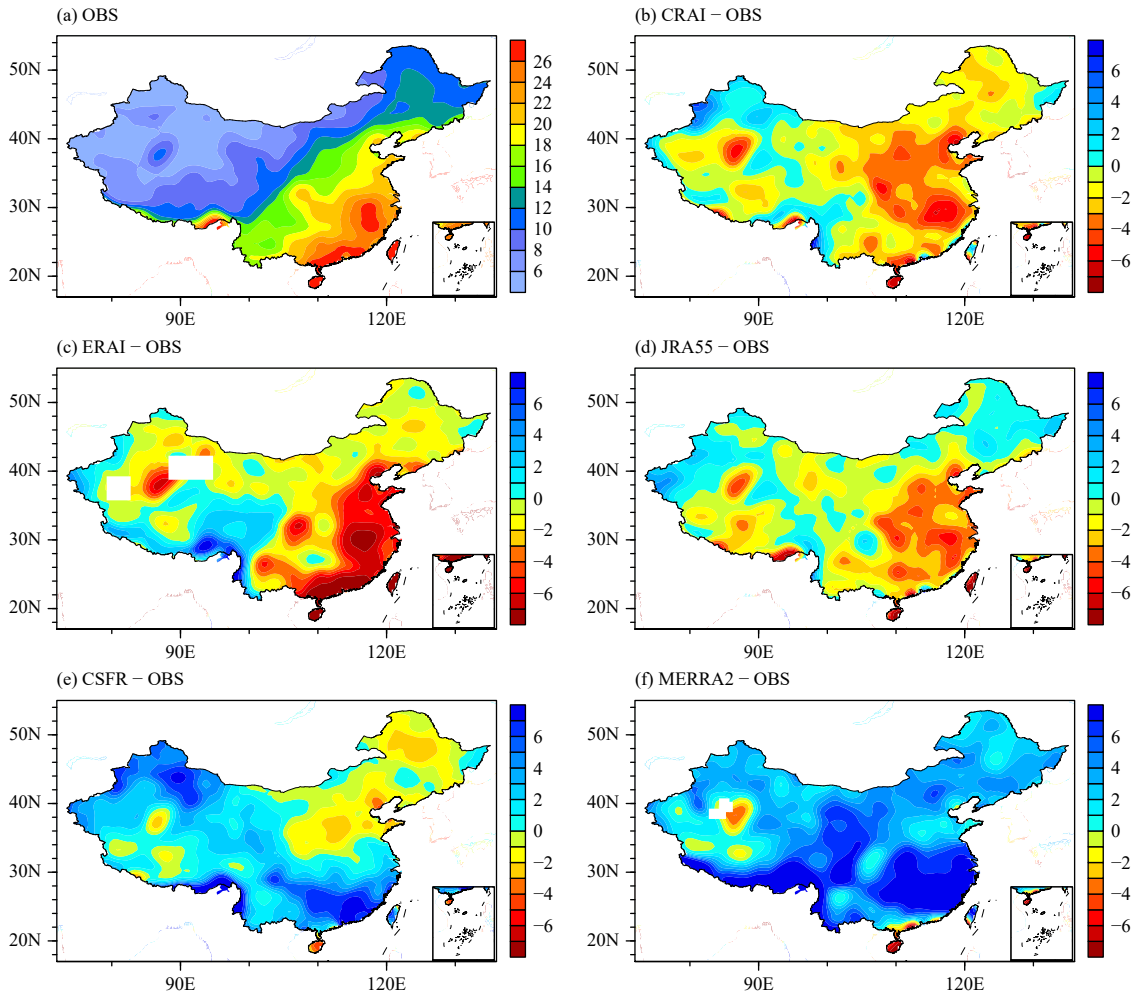

Fig. 8. The 95th percentiles of daily precipitation (mm day^{-1}) in (a) the observations (OBS), and the differences between the reanalysis datasets (b) CRAI, (c) ERAI, (d) JRA55, (e) CFSR, and (f) MERRA2 and OBS during 2007–2016. White shading indicates missing data.

events in China. Figure 8 shows the R95p of daily precipitation from 2007 to 2016. Here, R95p is the 95th percentile of daily precipitation on wet days (days with daily precipitation ⩾ 1 mm) and is used for defining extreme precipitation amounts. The maximum values of annual R95p for observations exceeding 26 mm day^{-1} are located along the southeast coast and over the lower reaches of the Yangtze River (Fig. 8a). Meanwhile, these values range between 18 and 26 mm day^{-1} in most parts of eastern China. Moreover, they decrease to 8–14 mm day^{-1} in most parts of central and eastern Inner Mongolia, the east of Northwest China, and Tibet, and become less than 6 mm day^{-1} in the west of Northwest China (Zhai et al., 2005). In general, the reanalyses capture a spatial distribution of R95p similar to that of the observational data, with values decreasing from south to north and east to west (figure omitted). However, CRAI, ERAI, and JRA55 tend to noticeably underestimate the high-value percentile indices (R95p ⩾ 18 mm day^{-1}) for humid regions in most parts of eastern China (Figs. 8b–d), where the annual precipitation amount (P) is more than 800 mm (Chen and Sun, 2015). By contrast, an overestimation of R95p is found in the southwestern China in ERAI. Moreover, overestimation extends from northwestern to southeastern China in CFSR (Fig. 8e) and throughout the entire country in MERRA2 (Fig. 8f).

The mean differences (bias), temporal correlations, and linear trends of R95pTOT are evaluated in Figs. 9–11, respectively. Since the daily precipitation in parts of northwestern China is below the threshold (R95p), blank spaces occur on the monthly correlation and trend analysis map. R95pTOT, derived from the observational data, shows a similar distribution to R95p (Fig. 8a), with more R95pTOT in Southeast China and less in Northwest China (Fig. 9a). The R95pTOT is underestimated by CRAI, ERAI, and JRA55 in southeastern China, indicating fewer instances of extreme precipitation there. However, the R95pTOT is generally overestimated by

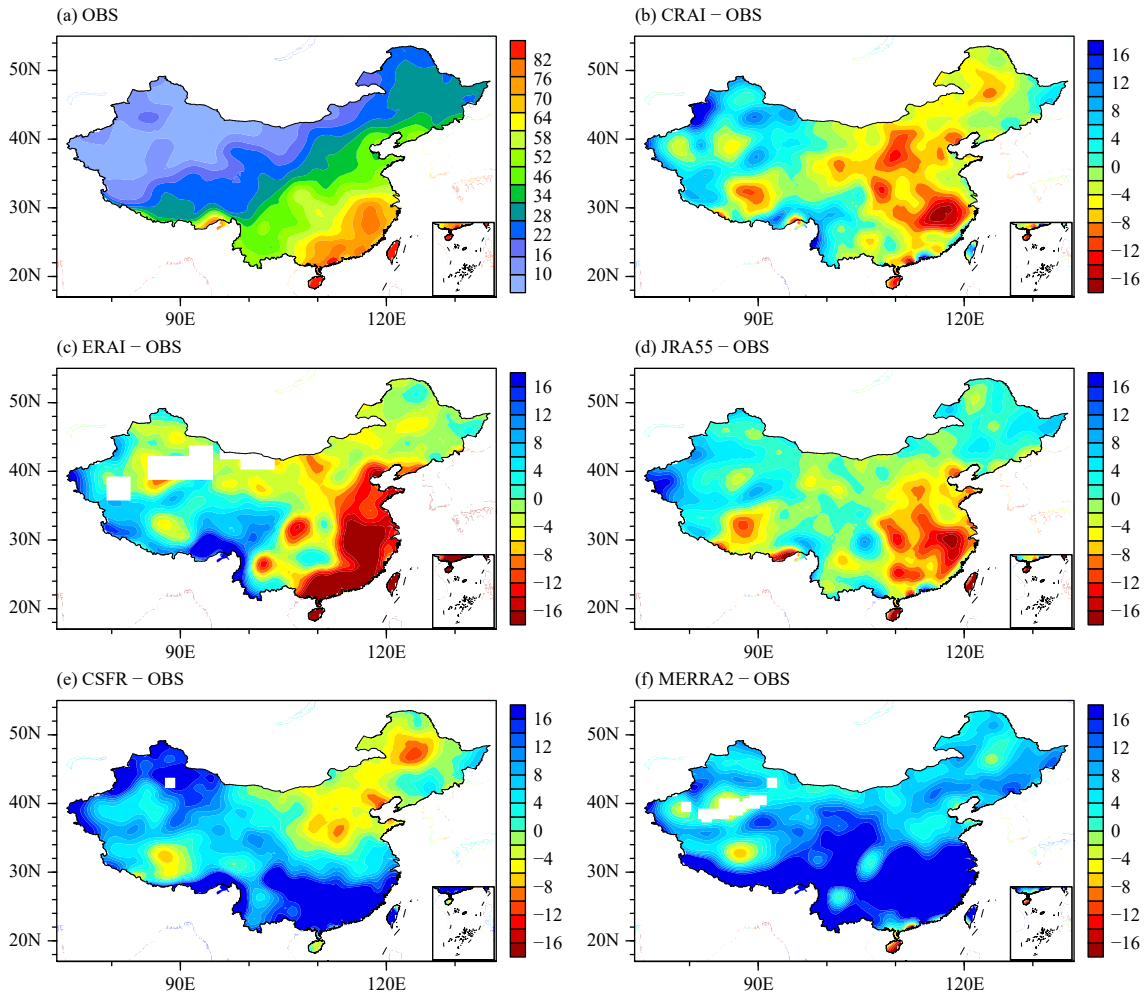

Fig. 9. Mean monthly R95pTOT (mm day^{-1}) from (a) the observations (OBS), and the differences between the reanalysis datasets (b) CRAI, (c) ERAI, (d) JRA55, (e) CFSR, and (f) MERRA2 and OBS during 2007–2016. White shading indicates missing data.

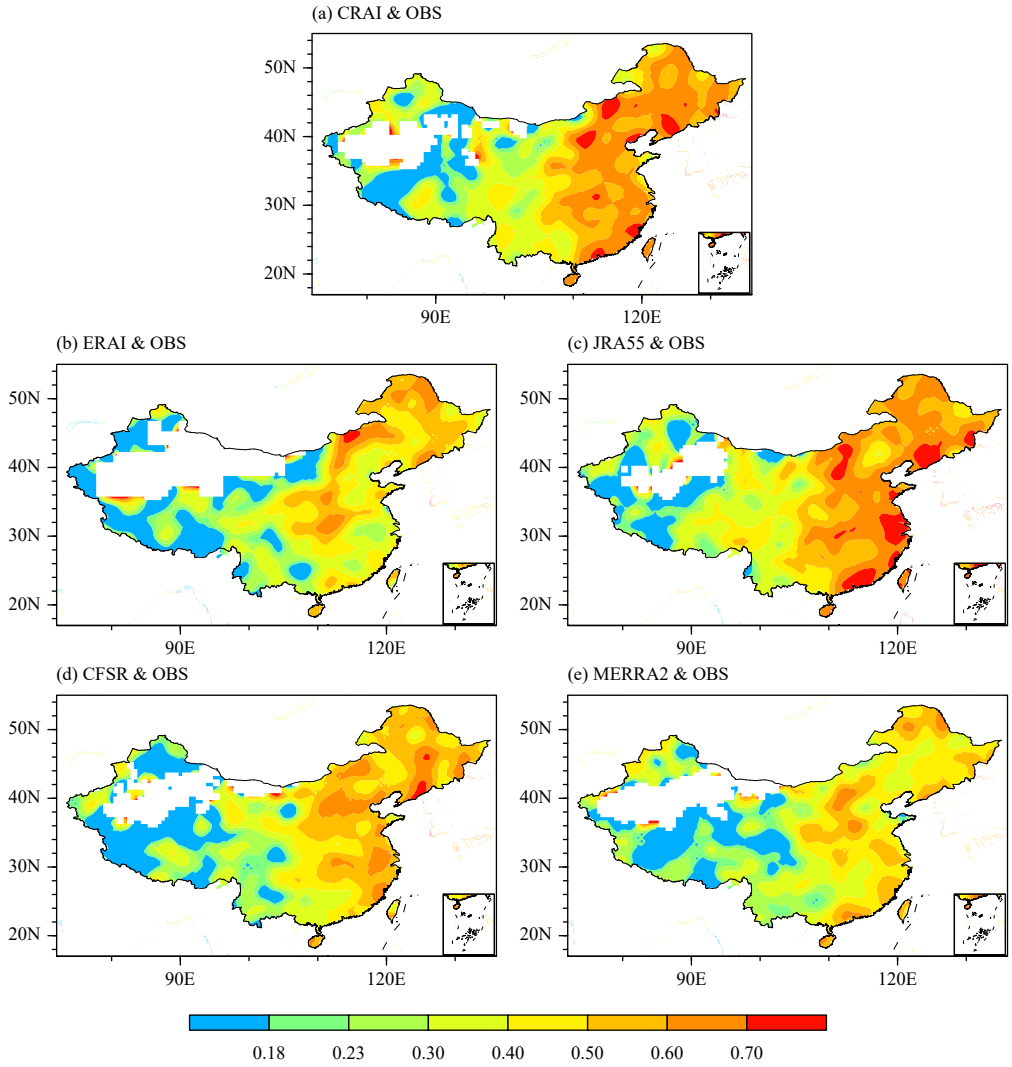

Fig. 10. Serial correlation coefficients (shading) of the monthly anomaly of R95pTOT between the reanalysis datasets (a) CRAI, (b) ERAI, (c) JRA55, (d) CFSR, and (e) MERRA2 and the observations (OBS) during 2007–2016. The values greater than 0.18 are significant at the 95% confidence level with a sample number of 120. White shading indicates missing data.

CFSR, with the exception of Northeast China (Fig. 9e). For MERRA2, consistent overestimation is found in China, and the maximum positive biases are located in southern China (Fig. 9f), which is similar to that of CFSR. That is, more frequent heavy rainfall can be found in most regions of China in both CFSR and MERRA2. These findings confirm the results shown in the histogram (Fig. 4), i.e., extreme precipitation is underestimated by CRAI, ERAI, and JRA55 but overestimated by CFSR and MERRA2.

With respect to the correlation coefficients between the reanalyses and the observational data for R95pTOT, high correlations are also observed in the southern and eastern regions of the country, where rain gauge networks are much denser and where extreme heavy rainfall events occur more frequently. In contrast, except for several small regions (e.g., in the northwestern corner of the country), the temporal variations of R95pTOT are poorly reproduced in western China. The corresponding correlation coefficients are close to zero or even negative (Fig. 10). In terms of linear trends, the observational data show that the monthly R95pTOT increases in Southeast and Northeast China and along the southern edge of the TP. All of the reanalyses can reproduce some features of R95pTOT change, with the pattern correlation coefficient of the trend ranging from 0.16 to 0.46. Nevertheless, the drying trend in the southwest from ERAI (Fig. 11c) is opposite to that of the observational data (Fig. 11a), while the wetting trend along the southern edge of the TP and Southeast China from both CFSR (Fig. 11e) and MERRA2 (Fig. 11f) is much more obvious than that seen in the observational data.

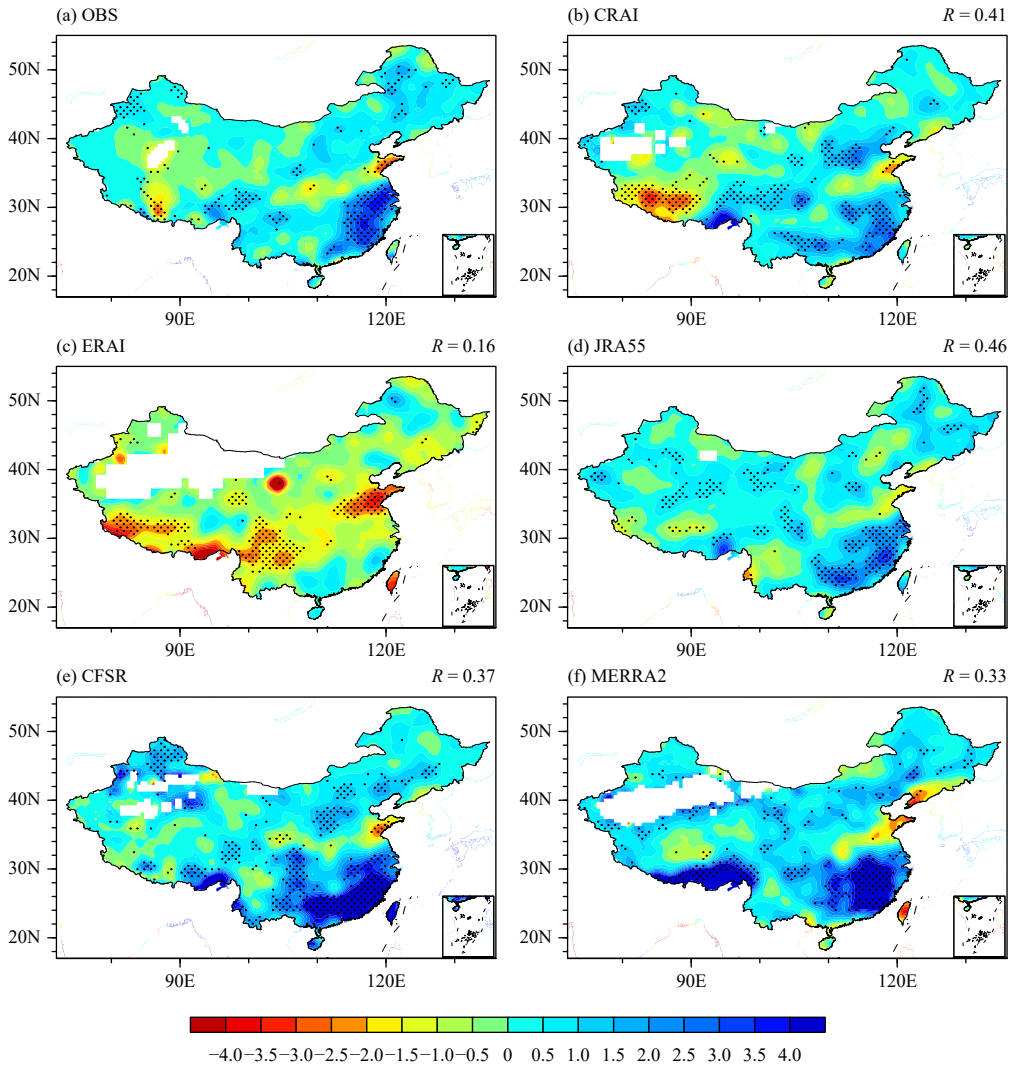

Fig. 11. Monthly R95pTOT trend [shading; mm day^{-1} (10 yr)$^{-1}$] during 2007–2016 from (a) the observations (OBS), (b) CRAI, (c) ERAI, (d) JRA55, (e) CFSR, and (f) MERRA2. The pattern correlation coefficient (R) between the reanalysis dataset and OBS is indicated on the top right of the corresponding panel. The dotted areas indicate the values exceeding the confidence level of 90%. White shading indicates missing data.

The observed minimum CDD is below 8 days, occurring mainly in the Sichuan basin and increasing both southward and northward, while high CDD values can be seen in southern Xinjiang and northern TP, approaching 26 days per month (Fig. 12a; Duan et al., 2017). This distribution can be reproduced by all of the reanalyses (figure omitted); however, CDD is generally underestimated, especially for both the northern and southern edges of the TP (Figs. 12b–f). In the reanalysis products, compared to the observational data, the indication is that dry spells are shorter in most regions of China, with a nationwide average bias of −3.29 to −1.28 days (Table 3). Meanwhile, the reanalyses show a better similarity to the observational data, with higher correlation coefficients in the eastern portions of the country but lower correlation coefficients in TP regions (Fig. 13). During the past 10 years, a significant decrease in observed CDDs is apparent in Southeast, North, and Northeast China, as well as along the western edge of the TP and in northern Xinjiang, with small positive values in the rest of the regions (Fig. 14a). CRAI, JRA55, and MERRA2 reproduce the wetting trend, with pattern correlation coefficients of 0.22–0.32 (Figs. 14b, d, f). However, a significant increase in CDD occurs over the TP in CFSR (Fig. 14e) and extends to northeastern and central China in ERAI (Fig. 14c).

Overall, in terms of R95pTOT, CRAI, ERAI, and JRA55 (CFSR and MERRA2) exhibit a smaller (larger) amount of extreme precipitation with relatively strong correlations with observational data in the southern and eastern portions of China, where the landfall of typhoons and the seasonal migration of monsoons (Meiyu) introduce abundant rainfall. Moreover, CRAI and JRA55

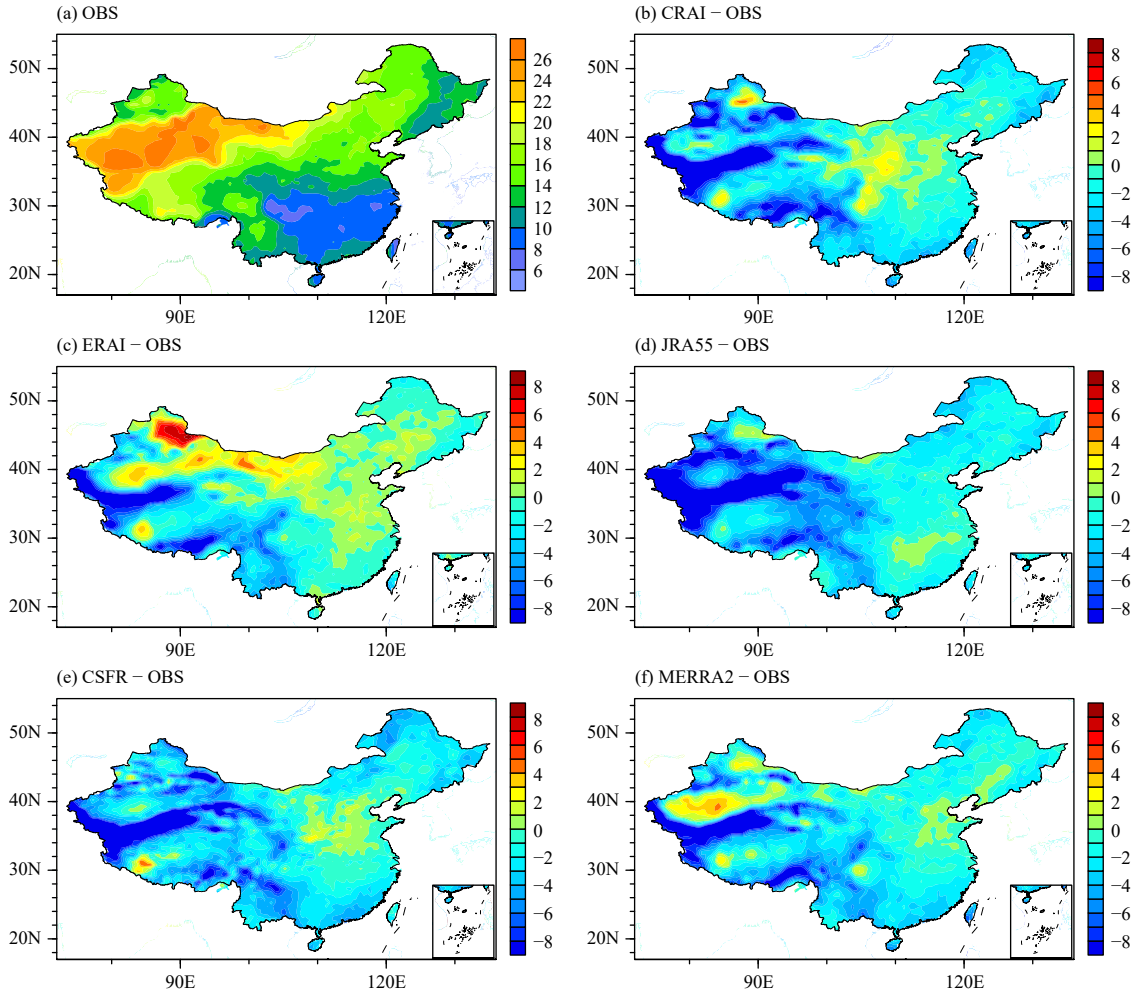

Fig. 12. As in Fig. 9, but for the monthly CDD (days).

Table 3. Anomaly biases and temporal correlation coefficients (Cor.) between the reanalysis products and observational data, as well as the linear trends in China for monthly R95pTOT (mm day^{-1}) and CDDs (days). The observed trends of R95pTOT and CDD are 0.41 mm day^{-1} (10 yr)$^{-1}$ and −0.08 days (10 yr)$^{-1}$, respectively

	R95pTOT			CDD		
	Bias	Cor.	Trend	Bias	Cor.	Trend
CRAI	−1.61	0.42	0.34	−2.93	0.54	−0.09
ERAI	−2.58	0.34	−0.79	−1.28	0.56	0.09
JRA55	−0.93	0.44	0.48	−3.79	0.54	−0.10
CFSR	6.67	0.35	1.05	−3.29	0.52	0.05
MERRA2	13.62	0.33	1.23	−2.59	0.56	−0.12

show better agreement with the observational data than the other products, with smaller biases (−1.61 and −0.93 mm day^{-1}), higher correlation coefficients (0.42 and 0.44), and much more similar linear trend patterns (the national average of the trend is 0.34 and 0.48 compared to 0.41 mm day^{-1} (10 yr)$^{-1}$ in observational data and 0.41 and 0.46 in pattern correlation coefficients). For CDD, all five reanalysis products underestimate the mean CDD duration, with fairly low correlations in the dry and arid regions of western China, where frequent droughts occur. Among them, ERAI stands out in capturing the amounts (bias of −1.28 days) and temporal variations of the observational data, with a national average correlation of 0.56. Although an opposite sign in the nationwide average trend is found in ERAI [0.09 versus −0.08 days (10 yr)$^{-1}$], it also performs better in depicting the spatial distribution of observed trends, with the pattern correlation coefficient of 0.39 (Fig. 14c).

3.3 *Comparison of moisture flux*

A possible explanation for the above mentioned biases might be related to the prevailing circulation. The

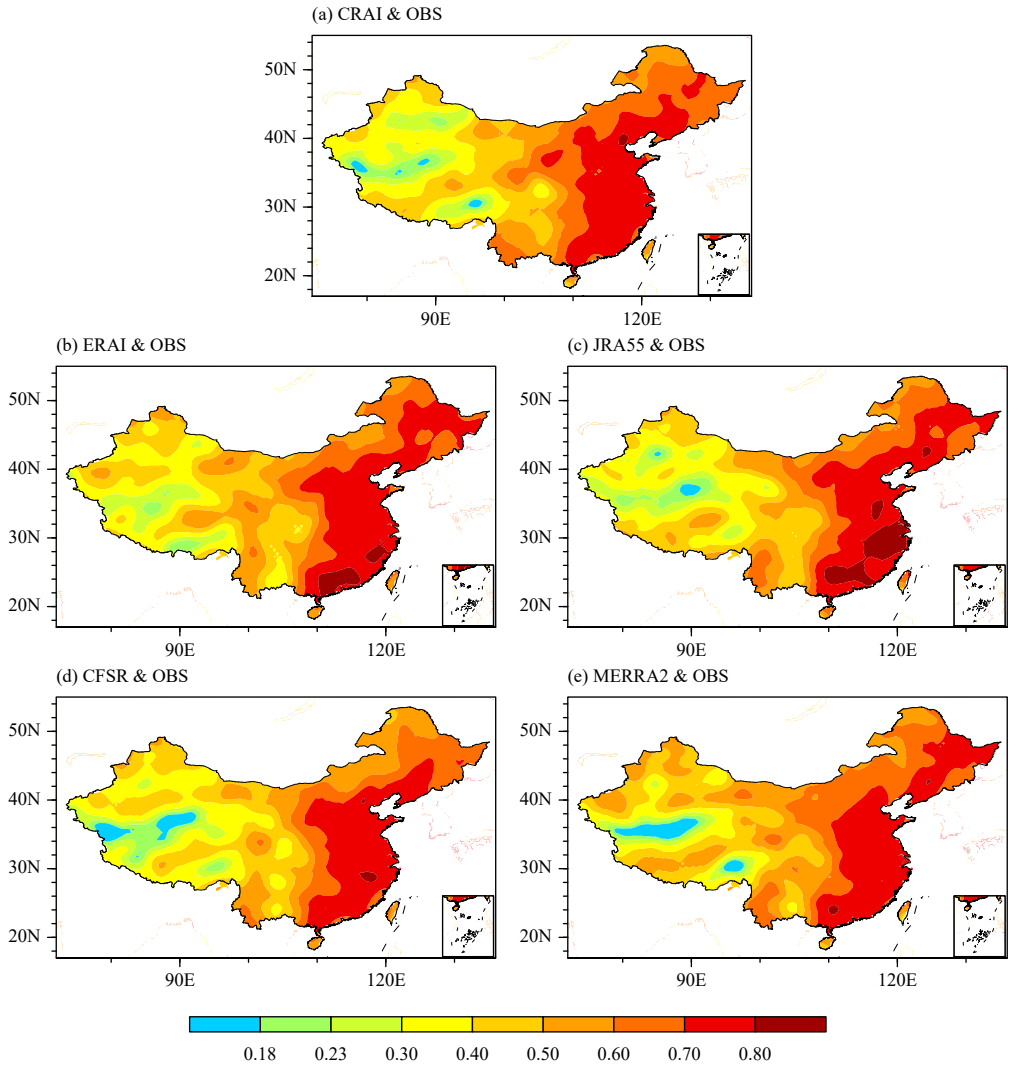

Fig. 13. As in Fig. 10, but for the monthly CDD.

differences in the seasonal mean precipitation and vertically integrated moisture flux and its divergence between CRAI and the other four reanalyses are shown in Supplementary Fig. S1 and Fig. S2, respectively. During the warm season, the vertically integrated moisture flux, in CRAI compared to CFSR and MERRA2, blows southward over eastern China and southern China, where this moisture flux is a crucial element in the development of thunderstorms that provide a substantial portion of both seasonal and extreme precipitation. Correspondingly, less seasonal mean precipitation (Supplementary Figs. S1e, g) and extreme precipitation (Figs. S9e, f) are found there. In comparison with ERAI and JRA55, northerly water vapor flux dominates northeastern China and central China, which then converges with the southwesterly flow over southwestern and southeastern China (Supplementary Figs. S2a, c) to result in insufficient precipitation in the former regions but sufficient precipitation in the latter regions (Supplementary Figs. S1a, c). Meanwhile, associated with an anomalous divergence of moisture over the TP (left-hand column of Supplementary Fig. S2), a dry bias is found there in CRAI compared to the other reanalysis products (left-hand column of Supplementary Fig. S2). During the cold season, CRAI shows a northward moisture flux in the eastern portion of China in comparison with CFSR and MERRA2 (Supplementary Figs. S2f, h), indicating a weakened winter monsoon, resulting in a decrease of precipitation there (Supplementary Figs. S1f, h).

4. Summary and discussion

In this study, we evaluate the capability of CRAI to capture the observed mean and spatiotemporal variability of precipitation, as well as extreme precipitation features, in China. The intercomparisons of reanalysis pre-

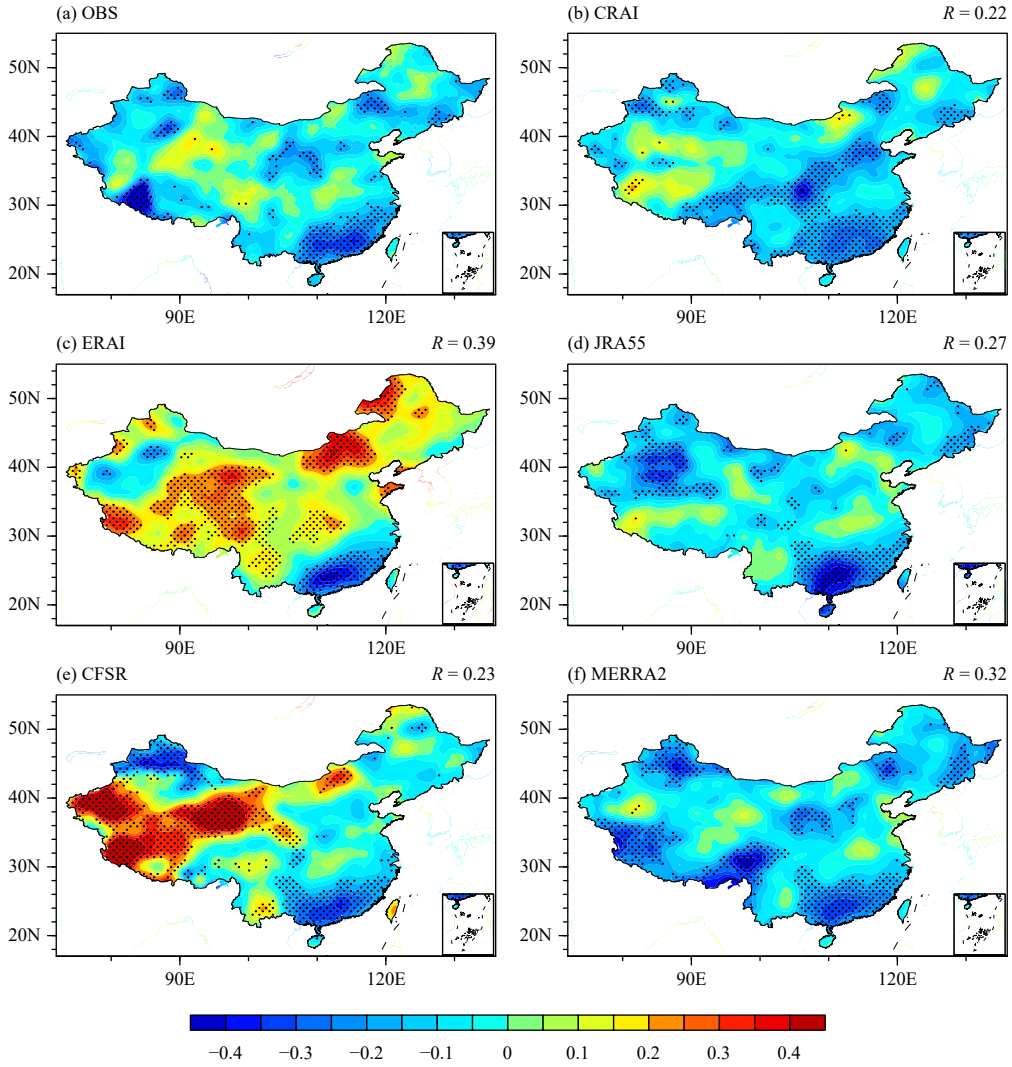

Fig. 14. As in Fig. 11, but for the monthly CDD [days (10 yr)$^{-1}$].

cipitation between CRAI, ERAI, JRA55, CFSR, and MERRA2, as well as the comparisons against observations, are performed for a 10-yr period from 2007 to 2016. The results show that the spatial characteristics, including the shape, orientation, and location of the precipitation area, as well as the seasonal and intraseasonal variations of precipitation, are generally reproduced by the five reanalyses. Furthermore, the performances of the reanalysis products vary for different regions and different precipitation regimes, with better performance in wet regions and for cold seasons. Among the reanalysis products, ERAI provides the best data on the magnitude of the 10-yr mean precipitation, while JRA55 exhibits the temporal variations and spatial patterns of precipitation closest to those of the observation data. Overall, the biases of the seasonal precipitation between the CRAI and other four reanalyses could be explained by the large-scale circulation and moisture fields.

For daily variations, all the reanalyses perform reasonably well in depicting the exact timing and location of rainfall bands, as well as the seasonal migration of precipitation bands, during the warm seasons in eastern China. However, both CFSR and CRAI exhibit stronger precipitation in the rain belt during the whole period, whereas the overestimation is confined to the south of 25°N in JRA55 but to the north of 24°N in MERRA2. For ERAI, an underestimation is found in most regions of eastern China, especially in the southern portions of South China during the whole period and in the lower reaches of the Yangtze River before late-July. An EOF analysis shows that the reanalysis products are reproduced well by the spatiotemporal evolution of the observed daily precipitation for most of China during the warm season. Among the reanalyses, JRA55 outperforms the other four reanalysis products in capturing the structure and variability of precipitation in warm seasons

in eastern China.

For extreme events, CRAI, ERAI, and JRA55 tend to underestimate the extreme precipitation amounts (R95pTOT), with relatively strong correlations with the observational data across most of eastern China, where the landfall of typhoons and the seasonal migration of monsoons (Meiyu) introduce abundant rainfall. In contrast, more frequent heavy rainfall can be found in most regions of China in both CFSR and MERRA2. Meanwhile, all of the reanalyses underestimate the CDDs, with fairly low correlations in the dry and arid regions of western China ($P < 200$ mm), where frequent droughts occur. Among them, CRAI and JRA55 show better agreement with the observed R95pTOT data than do the other products, with fewer biases, higher correlation coefficients, and much more similar linear trend patterns. Additionally, ERAI stands out in capturing the amount and temporal variations in the observed CDD data.

In general, CRAI, ERAI, and JRA55 tend to overestimate light and moderate grades of precipitation but underestimate heavy and extreme precipitation compared to the CPC observational data. Meanwhile, a bias of too much precipitation in all categories from light to extreme ranges is presented in both CFSR and MERRA2. Moreover, CRAI agrees best with the observed distribution of precipitation rates for the 8–25 mm day^{-1} range in China. These results suggest that CRAI is potentially applicable for studying the large-scale daily variability of precipitation in China, whereas it should be used with caution when monitoring heavy and extreme precipitation events in semi-humid ($400 \leqslant P < 800$ mm) and humid areas or the dry spells associated with droughts in arid and semi-arid ($200 \leqslant P < 400$ mm) areas of China. The results presented here suggest that various reanalysis products should be combined for the study of weather and climate, since no reanalysis product is superior to any other in terms of local-scale precipitation at daily timescales (Kidd and Huffman, 2011). Therefore, the application of reanalysis data for climate and hydrological studies should be performed carefully, and bias correction strategies are necessary for model initiation (Trenberth and Guillemot, 1998; Berg et al., 2003; Decker et al., 2012).

It is worth noting that these results are heavily dependent on the reliability of observations. However, there are many uncertainties in observed datasets, stemming from the quality and/or consistency of the underlying station data to the choices made within a chosen gridding/interpolation method (parametric uncertainty), and the network selection and analytical framework (structural uncertainty) (Yin et al., 2015). These uncertainties generally influence both the magnitude and trend of extreme precipitation (Hofstra et al., 2010). Hence, further analysis might be needed to test the robustness of the results using different observations. Moreover, how to improve the results is also not deeply dealt with in this study. Nevertheless, this study represents a comprehensive evaluation of the capability of the latest reanalysis products to capture the observed spatiotemporal variability of precipitation in China, including extreme precipitation events. The work provides an important reference for future climatic applications, including statistical flood frequency analysis, water resource planning, design, and system operations. In general, the CRAI precipitation data are applicable and interpretable. Further studies will compare CRAI with other observational data, such as gauge-observed daily precipitation records from a dense national network of > 2400 gauges, for clarifying the overall performance of the reanalysis. In addition, it would be desirable to carry out longer reanalyses by comparing the 40-yr product (CRA-40) with the recently released ERA5 reanalysis in the future work. More detailed analysis of the accuracy of daily data of CRAI will further explore the possible causes for the biases, in order to provide program developers with additional information that could lead to improvements.

Acknowledgments. The CFSR, MERRA2, and JRA55 were obtained from the NASA Center for Climate Simulation/Goddard Space Flight Center (https://esgf.nccs.nasa.gov/). The ERA-interim was obtained from the ECMWF Data Server at http://apps.ecmwf.int/datasets/.

REFERENCES

Alexander, L. V., X. Zhang, T. C. Peterson, et al., 2006: Global observed changes in daily climate extremes of temperature and precipitation. *J. Geophys. Res. Atmos.*, **11**, D05109, doi: 10.1029/2005JD006290.

Berg, A. A., J. S. Famiglietti, J. P. Walker, et al., 2003: Impact of bias correction to reanalysis products on simulations of North American soil moisture and hydrological fluxes. *J. Geophys. Res. Atmos.*, **108**, 4490, doi: 10.1029/2002JD003334.

Chen, G. X., T. Iwasaki, H. L. Qin, et al., 2014: Evaluation of the warm-season diurnal variability over East Asia in recent reanalyses JRA-55, ERA-interim, NCEP CFSR, and NASA MERRA. *J. Climate*, **27**, 5517–5537, doi: 10.1175/JCLI-D-14-00005.1.

Chen, H. P., and J. Q. Sun, 2015: Changes in drought characteristics over China using the standardized precipitation evapotranspiration index. *J. Climate*, **28**, 5430–5447, doi: 10.1175/JCLI-D-14-00707.1.

Chen, S., Y. Hong, Q. Cao, et al., 2013: Similarity and difference of the two successive V6 and V7 TRMM multisatellite precipitation analysis performance over China. *J. Geophys. Res.*

Atmos., **118**, 13060–13074, doi: 10.1002/2013JD019964.

Chen, T. C., 1985: Global water vapor flux and maintenance during FGGE. *Mon. Wea. Rev.*, **113**, 1801–1819, doi: 10.1175/1520-0493(1985)113<1801:GWVFAM>2.0.CO;2.

Committee for the Verification of Terms in Atmospheric Sciences, 2009: *Chinese Terms in Atmospheric Science*, 3rd ed., Science Press, Beijing, 14 pp. (in Chinese)

Dai, A. G., X. Lin, and K. L. Hsu, 2007: The frequency, intensity, and diurnal cycle of precipitation in surface and satellite observations over low- and mid-latitudes. *Climate Dyn.*, **29**, 727–744, doi: 10.1007/s00382-007-0260-y.

Dai, Z. J., R. C. Yu, J. Li, et al., 2011: The characteristics of summer precipitation diurnal variations in three reanalysis datasets over China. *Meteor. Mon.*, **37**, 21–30, doi: 10.7519/j.issn.1000-0526.2011.1.003. (in Chinese)

Decker, M., M. A. Brunke, Z. Wang, et al., 2012: Evaluation of the reanalysis products from GSFC, NCEP, and ECMWF using flux tower observations. *J. Climate*, **25**, 1916–1944, doi: 10.1175/JCLI-D-11-00004.1.

Dee, D. P., S. M. Uppala, A. J. Simmons, et al., 2011: The ERA-Interim reanalysis: Configuration and performance of the data assimilation system. *Quart. J. Roy. Meteor. Soc.*, **137**, 553–597, doi: 10.1002/qj.828.

Ding, Y. H., 1992: Summer monsoon rainfalls in China. *J. Meteor. Soc. Japan*, **70**, 373–396, doi: 10.2151/jmsj1965.70.1B_373.

Ding, Y. H., 1994: *Monsoons over China*. Kluwer Academic Publishers, Dordrecht, 419 pp.

Ding, Y. H., and J. C. L. Chan, 2005: The East Asian summer monsoon: An overview. *Meteor. Atmos. Phys.*, **89**, 117–142, doi: 10.1007/s00703-005-0125-z.

Donat, M. G., J. Sillmann, S. Wild, et al., 2014: Consistency of temperature and precipitation extremes across various global gridded in situ and reanalysis datasets. *J. Climate*, **27**, 5019–5035, doi: 10.1175/JCLI-D-13-00405.1.

Duan, Y. W., Z. G. Ma, and Q. Yang, 2017: Characteristics of consecutive dry days variations in China. *Theor. Appl. Climatol.*, **130**, 701–709, doi: 10.1007/s00704-016-1984-6.

Ebert, E. E., J. E. Janowiak, and C. Kidd, 2007: Comparison of near-real-time precipitation estimates from satellite observations and numerical models. *Bull. Amer. Meteor. Soc.*, **88**, 47–64, doi: 10.1175/BAMS-88-1-47.

Ferraro, R. R., 1997: Special sensor microwave imager derived global rainfall estimates for climatological applications. *J. Geophys. Res. Atmos.*, **102**, 16715–16735, doi: 10.1029/97JD01210.

Gao, X., Y. Shi, R. Song, et al., 2008: Reduction of future monsoon precipitation over China: Comparison between a high resolution RCM simulation and the driving GCM. *Meteor. Atmos. Phys.*, **100**, 73–86, doi: 10.1007/s00703-008-0296-5.

Gao, X. J., Y. Xu, Z. C. Zhao, et al., 2006: On the role of resolution and topography in the simulation of East Asia precipitation. *Theor. Appl. Climatol.*, **86**, 173–185, doi: 10.1007/s00704-005-0214-4.

Gao, Y. X., and S. Y. Xu, 1962: *Some Issues of the East Asian Monsoon*. Science Press, Beijing, 106 pp.

Guo, H., S. Chen, A. M. Bao, et al., 2016: Early assessment of integrated multi-satellite retrievals for global precipitation measurement over China. *Atmos. Res.*, **176–177**, 121–133, doi: 10.1016/j.atmosres.2016.02.020.

Hofstra, N., M. New, and C. McSweeney, 2010: The influence of interpolation and station network density on the distributions and trends of climate variables in gridded daily data. *Climate Dyn.*, **35**, 841–858, doi: 10.1007/s00382-009-0698-1.

Hubacek, K., D. B. Guan, and A. Barua, 2007: Changing lifestyles and consumption patterns in developing countries: A scenario analysis for China and India. *Futures*, **39**, 1084–1096, doi: 10.1016/j.futures.2007.03.010.

Isotta, F. A., R. Vogel, and C. Frei, 2015: Evaluation of European regional reanalyses and downscalings for precipitation in the Alpine region. *Meteorologische Zeitschrift*, **24**, 15–37, doi: 10.1127/metz/2014/0584.

Kidd, C., 2001: Satellite rainfall climatology: A review. *Int. J. Climatol.*, **21**, 1041–1066, doi: 10.1002/joc.635.

Kidd, C., and G. Huffman, 2011: Global precipitation measurement. *Meteor. Appl.*, **18**, 334–353, doi: 10.1002/met.284.

Kidd, C., and V. Levizzani, 2011: Status of satellite precipitation retrievals. *Hydrol. Earth Syst. Sci.*, **15**, 1109–1116, doi: 10.5194/hess-15-1109-2011.

Kirschbaum, D. B., G. J. Huffman, R. F. Adler, et al., 2017: NASA's remotely sensed precipitation: A reservoir for applications users. *Bull. Amer. Meteor. Soc.*, **98**, 1169–1184, doi: 10.1175/BAMS-D-15-00296.1.

Kobayashi, S., Y. Ota, Y. Harada, et al., 2015: The JRA-55 reanalysis: General specifications and basic characteristics. *J. Meteor. Soc. Japan*, **93**, 5–48, doi: 10.2151/jmsj.2015-001.

Kucera, P. A., E. E. Ebert, F. J. Turk, et al., 2013: Precipitation from space: Advancing earth system science. *Bull. Amer. Meteor. Soc.*, **94**, 365–375, doi: 10.1175/BAMS-D-11-00171.1.

Lin, R. P., T. J. Zhou, and Y. Qian, 2014: Evaluation of global monsoon precipitation changes based on five reanalysis datasets. *J. Climate*, **27**, 1271–1289, doi: 10.1175/JCLI-D-13-00215.1.

Luo, L. F., W. Tang, Z. H. Lin, et al., 2013: Evaluation of summer temperature and precipitation predictions from NCEP CFSv2 retrospective forecast over China. *Climate Dyn.*, **41**, 2213–2230, doi: 10.1007/s00382-013-1927-1.

Ma, L. J., T. J. Zhang, O. W. Frauenfeld, et al., 2009: Evaluation of precipitation from the ERA-40, NCEP-1, and NCEP-2 Reanalyses and CMAP-1, CMAP-2, and GPCP-2 with ground-based measurements in China. *J. Geophys. Res. Atmos.*, **14**, D09105, doi: 10.1029/2008JD011178.

Moberg, A., P. D. Jones, D. Lister, et al., 2006: Indices for daily temperature and precipitation extremes in Europe analyzed for the period 1901–2000. *J. Geophys. Res. Atmos.*, **111**, D22106, doi: 10.1029/2006JD007103.

Piao, S. L., P. Ciais, Y. Huang, et al., 2010: The impacts of climate change on water resources and agriculture in China. *Nature*, **467**, 43–51, doi: 10.1038/nature09364.

Rasmussen, R., B. Baker, J. Kochendorfer, et al., 2012: How well are we measuring snow: The NOAA/FAA/NCAR winter precipitation test bed. *Bull. Amer. Meteor. Soc.*, **93**, 811–829, doi: 10.1175/BAMS-D-11-00052.1.

Reichle, R. H., Q. Liu, R. D. Koster, et al., 2017: Land surface precipitation in MERRA-2. *J. Climate*, **30**, 1643–1664, doi: 10.1175/JCLI-D-16-0570.1.

Rudolf, B., A. Becker, U. Schneider, et al., 2010: The new "GPCC Full Data Reanalysis Version 5" providing high-qual-

ity gridded monthly precipitation data for the global land-surface is public available since December 2010. GPCC Status Report December 2010, GPCC, DWD, Germany, 1–7. Available online at https://www.dwd.de/EN/ourservices/gpcc/reports_publications/GPCC_status_report_2010.html?nn=495490. Accessed online 18 February 2020.

Saha, S., S. Moorthi, H. L. Pan, et al., 2010: The NCEP climate forecast system reanalysis. *Bull. Amer. Meteor. Soc.*, **91**, 1015–1057, doi: 10.1175/2010BAMS3001.1.

Shen, Y., A. Y. Xiong, Y. Wang, et al., 2010: Performance of high-resolution satellite precipitation products over China. *J. Geophys. Res. Atmos.*, **115**, D02114, doi: 10.1029/2009JD012097.

Sillmann, J., V. V. Kharin, X. Zhang, et al., 2013: Climate extremes indices in the CMIP5 multimodel ensemble: Part 1. Model evaluation in the present climate. *J. Geophys. Res. Atmos.*, **118**, 1716–1733, doi: 10.1002/jgrd.50203.

Su, Z. X., S. H. Lyu, and S. W. Luo, 1999: The examinations and analysis of NCEP/NCAR 40 years global reanalysis data in China. *Plateau Meteor.*, **18**, 209–218. (in Chinese)

Sun, Q. H., C. Y. Miao, Q. Y. Duan, et al., 2014: Would the 'real' observed dataset stand up? A critical examination of eight observed gridded climate datasets for China. *Environ. Res. Lett.*, **9**, 015001, doi: 10.1088/1748-9326/9/1/015001.

Trenberth, K. E., 1991: Climate diagnostics from global analyses: Conservation of mass in ECMWF analyses. *J. Climate*, **4**, 707–722, doi: 10.1175/1520-0442(1991)004<0707:CDFGAC>2.0.CO;2.

Trenberth, K. E., and C. J. Guillemot, 1998: Evaluation of the atmospheric moisture and hydrological cycle in the NCEP/NCAR reanalyses. *Climate Dyn.*, **14**, 213–231, doi: 10.1007/s003820050219.

Varis, O., and P. Vakkilainen, 2001: China's 8 challenges to water resources management in the first quarter of the 21st century. *Geomorphology*, **41**, 93–104, doi: 10.1016/S0169-555X(01)00107-6.

Wang, A. H., and X. B. Zeng, 2012: Evaluation of multi-reanalysis products with in situ observations over the Tibetan Plateau. *J. Geophys. Res. Atmos.*, **117**, D05102, doi: 10.1029/2011JD016553.

Xie, P. P., A. Yatagai, M. Y. Chen, et al., 2007: A gauge-based analysis of daily precipitation over East Asia. *J. Hydrometeor.*, **8**, 607–626, doi: 10.1175/JHM583.1.

Xie, P. P., M. Chen, and W. Shi, 2010: CPC unified gauge-based analysis of global daily precipitation. Proceedings of the 24th Conference on Hydrology, Atlanta, GA, American Meteorological Society.

Yin, H., M. G. Donat, L. V. Alexander, et al., 2015: Multi-dataset comparison of gridded observed temperature and precipitation extremes over China. *Int. J. Climatol.*, **35**, 2809–2827, doi: 10.1002/joc.4174.

Zhai, P. M., X. B. Zhang, H. Wan, et al., 2005: Trends in total precipitation and frequency of daily precipitation extremes over China. *J. Climate*, **18**, 1096–1108, doi: 10.1175/JCLI-3318.1.

Zhang, X. B., L. Alexander, G. C. Hegerl, et al., 2011: Indices for monitoring changes in extremes based on daily temperature and precipitation data. *WIREs Climate Change*, **2**, 851–870, doi: 10.1002/wcc.147.

Zhao, T. B., and C. B. Fu, 2006: Preliminary comparison and analysis between ERA-40, NCEP-2 reanalysis and observations over China. *Climatic Environ. Res.*, **11**, 14–32, doi: 10.3969/j.issn.1006-9585.2006.01.002. (in Chinese)

Zhao, T. B., and A. Yatagai, 2014: Evaluation of TRMM 3B42 product using a new gauge-based analysis of daily precipitation over China. *Int. J. Climatol.*, **34**, 2749–2762, doi: 10.1002/joc.3872.

Zhou, T. J., 2003: Comparison of the global air–sea freshwater exchange evaluated from independent datasets. *Prog. Nat. Sci.*, **13**, 626–631, doi: 10.1080/10020070312331344150.

Zhou, X. X., Y. H. Ding, and P. X. Wang, 2010: Moisture transport in the Asian summer monsoon region and its relationship with summer precipitation in China. *Acta Meteor. Sinica*, **24**, 31–42.

Tech & Copy Editor: Hongqun ZHANG